Journal of Alloys and Compounds 898 (2022) 162951

Contents lists available at ScienceDirect

Journal of Alloys and Compounds

journal homepage: www.elsevier.com/locate/jalcom

Effect of strain rate on fracture reliability of $Cu_{45}Zr_{45}Co_{10}$ amorphous alloy microwires by statistical analyses

Shuang Su[a,b], Zhiliang Ning[a,b], Yongjiang Huang[a,b,*], Tao Yang[c], Keyan Wang[a,b], Minqiang Jiang[d,f,**], Jianfei Sun[a,b], Sida Jiang[e,b,***]

[a] School of Materials Science and Engineering, Harbin Institute of Technology, Harbin 150001, China
[b] National Key Laboratory for Precision Hot Processing of Metals, Harbin Institute of Technology, Harbin 150001, China
[c] Department of Mechanical Engineering, City University of Hong Kong, Hong Kong, China
[d] State Key Laboratory of Nonlinear Mechanics, Institute of Mechanics, Chinese Academy of Sciences, Beijing 100190, China
[e] Space Environment Simulation Research Infrastructure, Harbin Institute of Technology, Harbin 150001, China
[f] School of Engineering Science, University of Chinese Academy of Sciences, Beijing 100049, China

ARTICLE INFO

Article history:
Received 15 September 2021
Received in revised form 29 October 2021
Accepted 23 November 2021
Available online 26 November 2021

Keywords:
Amorphous alloy microwires
Strain rate effect
Fracture strength
Fracture reliability
Statistical analyses

ABSTRACT

The understanding of the fracture mechanism of amorphous alloys (AAs) is of importance for their engineering applications as advanced structural materials. In this study, a series of micro-tensions of $Cu_{45}Zr_{45}Co_{10}$ AA microwires were conducted under different strain rates ranging from 5×10^{-5} s^{-1} to 1×10^{-2} s^{-1}. It is found that all microwires fracture by shear cracking, but the shear fracture strengths exhibit pronounced rate-dependent uncertainties. Based on both lognormal and Weibull statistical analyses, the studied AA microwires reveal a positive rate-sensitivity of fracture strengths. However, increasing strain rates incurs the decrease in the fracture reliability. We demonstrate that the fracture reliability of AA microwires is dominated by a square root singularity of the characteristic lengths of shear offset on fracture surfaces, which satisfies linear elastic fracture mechanics.

1. Introduction

Different from traditional metallic materials, amorphous alloys (AAs) lack a dislocation-based plastic deformation mechanism, which results in high strength approaching the theoretical limit [1–5]. AA microwires have tunable sample diameters, uniform structure, few casting defects, and high replicability [6–8], and therefore are an ideal system to study deformation behaviors of amorphous solids. During the past decades, tremendous efforts have been devoted to processing AA microwires under high cooling rates and characterizing their mechanical properties [9,10]. For instance, Wang et al. [11] reported the submicron-sized $Pd_{40}Cu_{30}Ni_{10}P_{20}$ AA microwires with an ultrahigh tensile strength up to ~2.8 GPa, almost twice as high as that of bulk counterparts. Owing to their excellent mechanical properties, AA microwires are promising materials for potential structural applications in micro/nano-electro-mechanical systems (MEMS) [12,13]. These promising applications require a deep understanding of the mechanical properties and evolutionary mechanism of AA microwires [14–16].

Statistical analysis is a commonly used method for studying structural defects of brittle materials and has been recently applied for the mechanical characterization of AAs [17,18]. For instance, Qin et al. [19] analyzed the tensile strength of Gd-based AA microwires using the Weibull and lognormal statistics, showing that the mean tensile strength and fracture strain were ~1200 MPa and ~2.0%, respectively. It should be also noticed that deformation behavior of AAs is largely affected by imposed loading conditions such as strain rate [20]. Researchers demonstrated a positive strain rate dependence of compressive yielding strength in Ti-based bulk amorphous alloys (BAAs) [21,22]. Contrarily, Sort et al. [23] showed a negative rate sensitivity of mechanical properties in Ti-based BAAs. Similar inconsistent results have been also reported in Ni-based and Mg-based AAs [24,25]. Obviously, the mechanical properties of some AAs are sensitive to applied tensile strain rate. Although the strain rate sensitivity of the mechanical behaviors of AA has recently triggered

* Corresponding author at: School of Materials Science and Engineering, Harbin Institute of Technology, Harbin 150001, China.
** Corresponding author at: State Key Laboratory of Nonlinear Mechanics, Institute of Mechanics, Chinese Academy of Sciences, Beijing 100190, China.
*** Corresponding author at: Space Environment Simulation Research Infrastructure, Harbin Institute of Technology, Harbin 150001, China.
E-mail addresses: yjhuang@hit.edu.cn (Y. Huang), mqjiang@imech.ac.cn (M. Jiang), jiangsida@hit.edu.cn (S. Jiang).

https://doi.org/10.1016/j.jallcom.2021.162951
0925-8388/

intense attention in materials science community [26], most of these studies focused on the effect of the applied strain rates on their fracture strength and structural evolutions. Actually, due to the characteristic of structural inhomogeneity, brittle AA microwires do not exhibit identical deformation and fracture behaviors even though at the same strain rate, leading to the scattered fracture strength values [27–30]. The dispersion degree of strength values determines the fracture reliability of AA microwires, which is critical for the long-term industrial applications of structural materials. Generally, the fracture strength is closely related to fracture morphology [31]. Therefore, it is of scientific and technological importance to establish underlying relations among strain rate, fracture strength, fracture reliability, and fracture morphology, which will facilitate a better understanding of the deformation mechanism of AA microwires.

Here, we choose $Cu_{45}Zr_{45}Co_{10}$ (at%) AA microwires as the model materials and perform the uniaxial tensile loading tests over a wide range of strain rates from 5×10^{-2} s^{-1} to 5×10^{-5} s^{-1}. Lognormal and Weibull statistical analyses of the tensile fracture strength were carried out. Fitting parameters of the models were explored in details to illustrate the effect of tensile strain rate on mechanical behaviors of AA microwires. Based on the careful observations of fracture surfaces of AA samples, the quantitative relationship between shear offset lengths and fracture strengths was established. The combination of statistical analyses and experimental data provided significant insights into the deformation mechanism of CuZr-based AA microwires. It is expected that the results obtained in this study will lay a solid theoretical basis for exploring the mechanical behaviors and the related influencing factors of AA microwires.

2. Experimental procedures

The master alloy ingots with a nominal chemical composition of $Cu_{45}Zr_{45}Co_{10}$ were prepared by arc melting high-pure Cu, Zr, and Co metals in an arc furnace under an inert (pure Ar) atmosphere. To ensure chemical homogeneity, the remelting of each ingot was repeated at least four times under pure Ar atmosphere. Then, the alloy was cast into a copper mold to produce cylindrical rods with 10 mm in diameter and 50 ± 10 mm in length. The rods were further extracted by a home-made melt-extracted device made of a boron nitride (BN) crucible and a high-frequency induction coil for alloy remelting (Fig. 1). The melt was extracted by a rotating Cu wheel with a constant linear velocity of 30 $m{\cdot}s^{-1}$ and a feeding rate of 30 $\mu m{\cdot}s^{-1}$. The resulting microwires have a diameter ranging from 20 to 50 μm. The details for sample preparation procedures have been provided in Ref. [32]. To avoid the effect of sample sizes on mechanical behaviors of AA microwires [33], the samples with a smooth surface and negligible fluctuation in diameter size of 40 ± 1 μm were selected from the abundant as-cast microwires before tests.

The structure of AA microwires was characterized by X-ray diffractometer (XRD) with Cu K_α radiation (type: X'PERT), and a high-resolution transmission electron microscope (TEM, type: Talos F200X). The samples for TEM observations were prepared using an ion milling operated at 4.5 KeV to ensure electron transparency. The thermal properties were performed using a Perkin-Elmer differential scanning calorimeter (DSC, type: STA449F3) at the constant heating rate of 20 K min^{-1} in a flow of purified argon gas. The geometry of AA microwires and fracture morphologies were observed by a scanning electron microscope (SEM, type: HELIOS NanoLab 600i). Tensile samples were prepared following the ASTM standard D3379–75 with a gauge length of 8 mm. To facilitate measurement, the microwire was fixed between two pieces of paperboard with super glue. The paperboard shape is schematically illustrated in the inset of Fig. 1, with an overall length of 40 mm and a width of 20 mm. Micro-tension experiments of AA microwires were conducted on a 10 N Instron 3343 universal testing machine at room temperature under the following strain rates: 5×10^{-2} s^{-1}, 1×10^{-2} s^{-1}, 5×10^{-3} s^{-1}, 1×10^{-3} s^{-1}, 5×10^{-4} s^{-1}, 1×10^{-4} s^{-1}, 5×10^{-5} s^{-1}, and 1×10^{-5} s^{-1}, respectively. In order to facilitate statistical analysis of the mechanical properties, twelve microwire samples were tested at each strain rate. Totally, 96 samples were tested and quantitatively analyzed. The fracture strengths of AA microwires were subsequently analyzed using lognormal and Weibull statistics methods.

3. Results

Fig. 2(a) shows the SEM image of the extracted AA microwires. As seen, the AA microwires have smooth and round shape, and uniform diameter. Fig. 2(b) shows the XRD pattern of the extracted AA microwires. The broad XRD peak at $2\theta = 38°$ and the absence of any other peaks originating from the sharp-edged crystal lattice demonstrate fully amorphous structure of the melt-extracted microwires. In order to further characterize the structure of melt-extracted AA microwires, TEM observations were performed. Fig. 2(c) shows the corresponding high resolution TEM (HRTEM) image and selective area electron diffraction (SAED) pattern (inset). The AA microwire possesses a featureless structure without any long-range atomic configuration, typical of amorphous structure. The monolithic amorphous phase was also verified by a single halo ring (see SAED pattern in Fig. 2(c) inset). The amorphous structure of

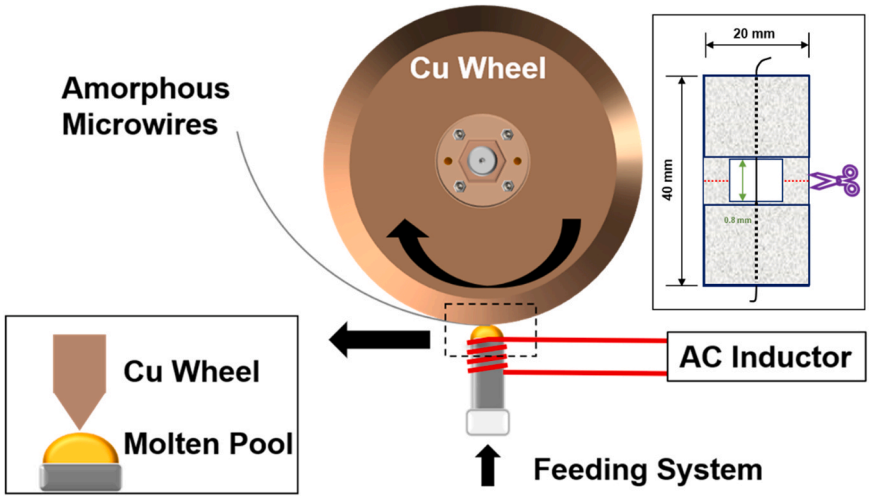

Fig. 1. Schematic representation of melt-extraction setup. The inset illustrates the shape of tensile test sample.

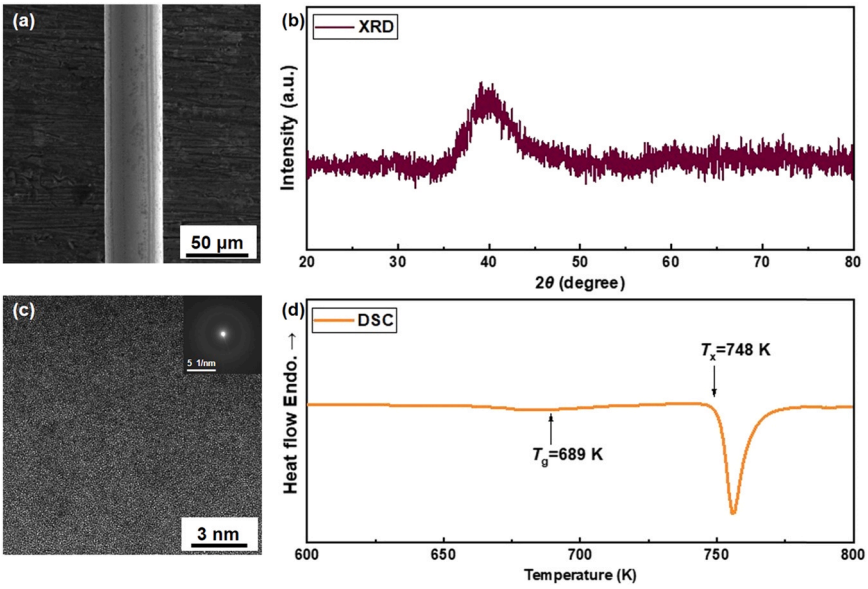

Fig. 2. (a) SEM image, (b) XRD pattern, (c) HRTEM image and SAED pattern (inset), and (d) DSC curve of $Cu_{45}Zr_{45}Co_{10}$ amorphous alloy microwires.

microwires is ensured by the high cooling rate during the extraction process, which can go up to 10^6 K·s^{-1}, far beyond the critical value (about 10^3 K·s^{-1}) required for the formation of CuZr-based AAs. The DSC curve (Fig. 2(d)) revealed the existence of an endothermic glass transition process with a glass transition temperature (T_g) of 689 K, and an exothermic crystallization process at the crystallization temperature (T_x) of 748 K.

The tensile tests of the AA microwires were carried out under various strain rates at room temperature. The corresponding stress-strain curves of the AA microwires are shown in Fig. 3(a)-(h). The fracture strengths at each strain rate as well as their range values are listed in Table 1. With the strain rate slowing down from 5×10^{-2} s^{-1} to 1×10^{-5} s^{-1}, the maximum values of fracture strength decrease from 2577 MPa to 1985 MPa, while its minimum values also show a downward trend from 1495 MPa to 1402 MPa, which suggests positive strain rate sensitivity of fracture strength for the studied AA microwires. Furthermore, as strain rate decreases, the range, defined as the increment between the maximum and minimum fracture strength, gradually decreases from 1082 MPa to 583 MPa, indicating a reduction of dispersion degree in fracture strength values. No apparent plastic deformation can be observed in each curve, suggesting a brittle deformation feature of AA microwires. The maximum fracture strength of $Cu_{45}Zr_{45}Co_{10}$ AA microwires (2577 MPa at the strain rate of 5×10^{-2} s^{-1}) is much higher than that of bulk one (1890 MPa) [34], which might be associated with the highly uniform structure of melt-extracted AA microwires [35].

To quantitatively assess the deviations in fracture strength of brittle AA microwires (Fig. 3), two statistical analyses methods were employed. In logarithmic distribution method, the probability for fracture under the applied stress conditions, P_i^{LN}, is given by the following formula [36].

$$P_i^{LN} = \frac{1}{2}\left[1 + erf\left(\frac{\ln(\sigma) - \kappa}{s\sqrt{2}}\right)\right] \quad (1)$$

where i represents the sample number, σ denotes the applied uniaxial stress, κ is the mean value, and s is the standard deviation of $\ln\sigma$ values. The parameter κ can be calculated as $\ln(\sigma_0)$, where σ_0 stands for the geometric mean value of fracture strengths.

The simplified method for calculating the failure probability P_i^{LN} under a given σ_i is based on a median rank value and the experimental data are shown in Table 1:

$$P_i^{LN} = \frac{i - 0.3}{N + 0.4} \times 100\% \quad (2)$$

where N is the overall number of the testing samples.

Based on the values of fracture strength under each tensile strain rate, the fitting curves of logarithmic normal distribution models are shown in Fig. 4(a)-(h). From the graph of $\ln(\sigma)$ vs. $(2P_i^{LN}-1)$, the parameters κ, s, and σ_0 could be obtained. The fitted parameters for geometric and arithmetic average Fig. 5 strength for the strain rates between 5×10^{-2} s^{-1} to 1×10^{-5} s^{-1} are compared in Fig. 6(a). The relevant data are listed in Table 1. Both parameters decrease as the applied strain rate decreases. Moreover, geometric average strength declines more rapidly than the arithmetic average strength values, and the two parameters reach almost the same values at the lowest strain rate of 1×10^{-5} s^{-1}. Fig. 6(b) reveals that the standard deviation s also shows a decreasing trend as the strain rate goes from 5×10^{-2} s^{-1} down to 1×10^{-5} s^{-1}, which illustrates that the dispersion of fracture strength gets lower as the strain rate decreases.

Weibull statistical model is also a common method used alternatively for the evaluation of probability failure of brittle materials [37]. The cumulative failure probability is expressed by the following formula [37].

$$P_i^{WB} = 1 - exp\left[-V\left(\frac{\sigma - \sigma_\mu}{\sigma_p}\right)^m\right] \quad (3)$$

where V represents the volume of the material, σ_μ denotes the minimum stress required to cause a fracture, σ_p is the Weibull parameter that is the stress when P_i^{WB} reaches 63.2%, and m is the Weibull modulus that represents the variability of the mechanical strength, where narrower probability distribution graphs have higher m values. Eq. (3) is usually transformed into a three-parameter Weibull model (TrPWM) as follows:

$$\ln\left[\ln\left(\frac{1}{1 - P_i^{WB}}\right)\right] = m_{Tr}\ln(\sigma - \sigma_\mu) - m_{Tr}\ln\sigma_0 \quad (4)$$

The threshold stress σ_μ, where there is no fracture probability, is usually taken for this model, and this corresponds to $\sigma_\mu = 0$ [38]. Therefore, the TrPWM is simplified into a two-parameter Weibull model (TPWM):

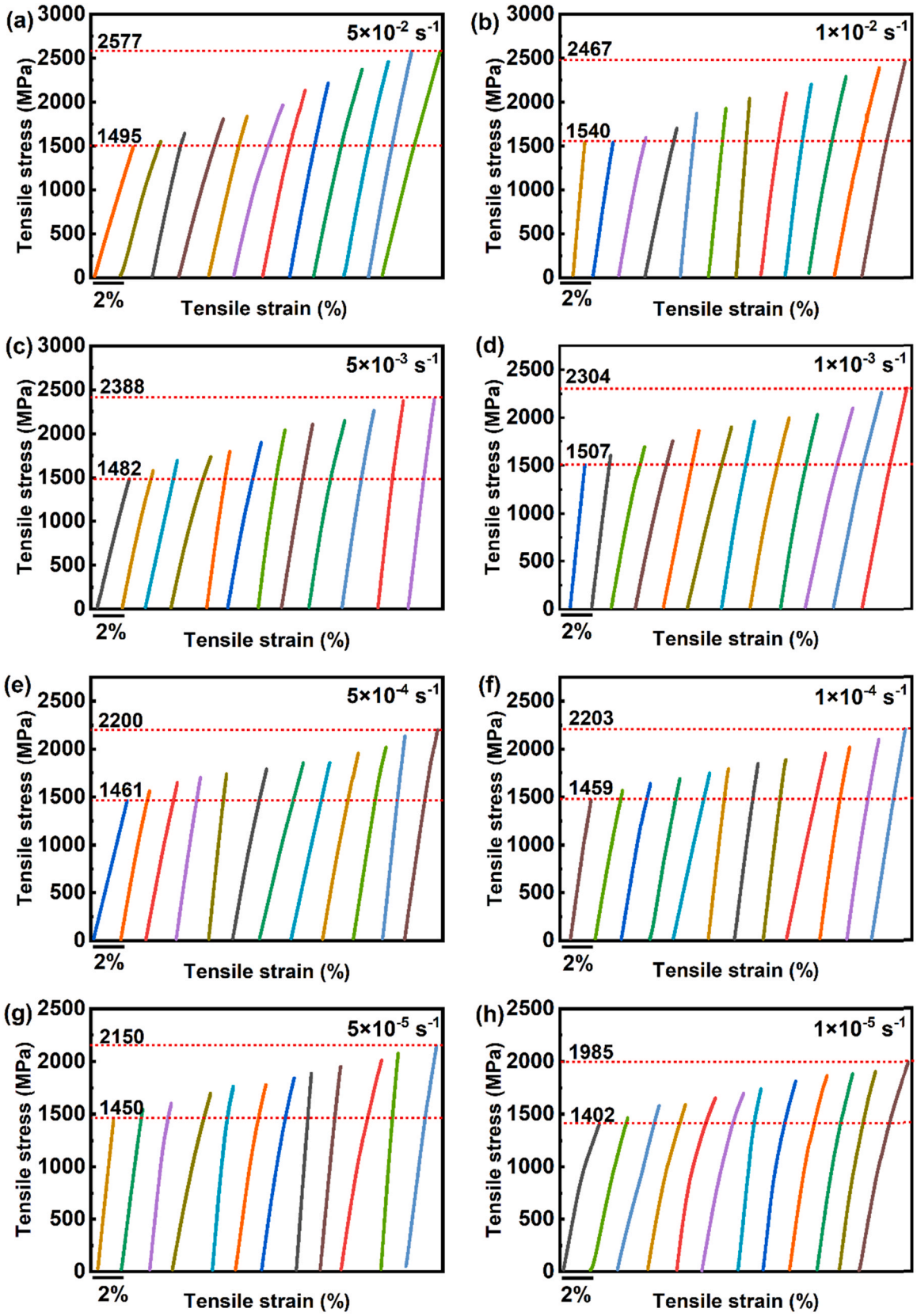

Fig. 3. Engineering stress-strain curves of $Cu_{45}Zr_{45}Co_{10}$ AA microwires at room temperature under different strain rates of (a) 5×10^{-2} s^{-1}, (b) 1×10^{-2} s^{-1}, (c) 5×10^{-3} s^{-1}, (d) 1×10^{-3} s^{-1}, (e) 5×10^{-4} s^{-1}, (f) 1×10^{-4} s^{-1}, (g) 5×10^{-5} s^{-1} and (h) 1×10^{-5} s^{-1}, respectively.

Table 1
Fracture strengths of $Cu_{45}Zr_{45}Co_{10}$ AA microwires under different strain rates and their ranges.

Strain rate (s^{-1})		5.0×10^{-2}		1.0×10^{-2}		5.0×10^{-3}		1.0×10^{-3}		5.0×10^{-4}		1.0×10^{-4}		5.0×10^{-5}		1.0×10^{-5}	
Fracture strength (MPa) & Length of shear offset (μm)		1495	24.2	1540	24.0	1482	25.9	1507	25.9	1461	27.9	1459	27.9	1450	28.4	1402	29.7
		1553	24.0	1543	23.0	1580	21.1	1610	23.1	1566	24.6	1570	24.5	1550	26.2	1465	28.7
		1642	20.8	1599	21.5	1694	20.5	1697	22.4	1651	22.8	1642	22.0	1602	24.4	1581	25.1
		1881	17.2	1704	16.2	1735	19.3	1757	17.8	1704	20.2	1693	21.5	1699	20.3	1593	22.7
		1842	15.7	1875	14.9	1801	16.6	1865	15.2	1742	19.1	1753	18.9	1765	19.5	1653	20.7
		1966	13.4	1927	14.0	1902	15.4	1905	14.4	1793	18.8	1797	16.7	1780	18.2	1699	20.3
		2137	12.9	2043	13.8	2043	13.8	1960	14.3	1860	17.3	1855	15.4	1844	17.7	1740	19.2
		2220	9.6	2102	11.9	2100	11.1	1999	12.6	1900	15.5	1889	15.7	1885	15.8	1815	18.3
		2373	8.4	2204	10.5	2148	10.2	2035	11.9	1957	14.3	1960	14.3	1953	14.4	1869	17.1
		2464	8.3	2294	9.3	2267	10.7	2102	11.9	2021	13.2	2020	13.2	2011	13.4	1882	15.8
		2576	7.1	2393	8.3	2375	9.4	2267	10.7	2137	11.4	2105	12.8	2078	12.3	1903	15.4
		2577	6.9	2467	7.0	2388	9.1	2304	9.2	2200	10.5	2203	11.5	2150	12.2	1985	12.8
Range (MPa)		1082		927		906		707		739		744		700		583	
Arithmetic average (MPa)		2055		1974		1959		1917		1832		1828		1813		1715	
Geometric average (MPa)		2030		1960		1946		1913		1824		1821		1812		1717	
Fracture threshold (MPa)		2218		2116		2090		2032		1929		1924		1907		1796	
Standard deviations (s)			0.234		0.202		0.187		0.144		0.134		0.134		0.133		0.122
Two-parameter modulus (m_T)			5.64		6.44		6.98		8.32		9.09		9.20		9.31		10.30
Three-parameter modulus (m_{Tr})			**1.58**		**1.91**		**2.21**		**2.85**		**3.05**		**3.17**		**3.51**		**4.33**

$$\ln\left[\ln\left(\frac{1}{1-P_i^{WB}}\right)\right] = m_T\ln(\sigma) - m_T\ln\sigma_0 \tag{5}$$

The Weibull modulus m_{Tr} in Eq. (4) has the same meaning as m_T in Eq. (5), indicating fracture reliability of materials. Fig. 6(c) shows the variation in m_T and m_{Tr} at different strain rates. The corresponding values are listed in Table 1. As seen, both m_T and m_{Tr} increase gradually with decreasing strain rate, suggesting enhanced fracture reliability and mechanical robustness at a slower strain rate. Fig. 6(d) shows the variation tendency of fracture threshold with strain rate changing. As seen, the decrease in strain rate from 5×10^{-2} s^{-1} to 1×10^{-5} s^{-1} brings the fracture threshold down from 2218 MPa to 1796 MPa. Therefore, the fracture threshold of $Cu_{45}Zr_{45}Co_{10}$ AA microwires shows positive sensitivity to strain rate in tensile tests. The above results are consistent with the results presented in Fig. 6(a).

4. Discussion

According to the shear transformation zone (STZ) theory, the plastic deformation of AA microwires is largely localized within shear bands of several tens of nanometers in thickness. At low temperature and high stress, the relationship between shear strain rate $\dot{\gamma}$ and the shear stress τ of AA microwires can be expressed by the following formula [39]:

$$\dot{\gamma} = \dot{\gamma}_G exp\left(-\frac{\Delta G - \tau V}{k_B T}\right) \tag{6}$$

where γ_G represents intrinsic strain rate ~ 10^{11} s^{-1}, V denotes the activation volume of STZ, ΔG is the Boltzmann's constant, and T is test temperature. The shear strength τ can be expressed as:

$$\tau = \left(\Delta G - k_B T In\frac{\dot{\gamma} G}{\dot{\gamma}}\right)/V \tag{7}$$

As can be seen, the shear stress of AAs is closely related to strain rate, STZ activation energy and temperature. Eqs. (6) and (7) can be combined and reformulated as:

$$\left(\frac{\partial\tau}{\partial\dot{\gamma}}\right)_{\Delta G,T} = \Delta G k_B/V\dot{\gamma} \tag{8}$$

Shear stress τ and fracture strength σ can be written as:

$$\sigma = \tau/\sin\theta\cos\theta \tag{9}$$

The shear strain rate and axial shear strain rate ε can be written as:

$$\varepsilon = \dot{\gamma}L\cos\theta/h \tag{10}$$

where h represents the sample length, L denotes the critical shear offset width, and θ is the sheared off angle. The relationship between fracture strength and axial shear strain rate can be expressed as:

$$\left(\frac{\partial\sigma}{\partial\varepsilon}\right)_{\Delta G,T} = \Delta G k_B/V\varepsilon > 0 \tag{11}$$

According to Eq. (11), a higher uniaxial tensile strain rate will result in a higher shear strain rate, thereby facilitating a greater strain rate hardening effect, and a higher fracture strength of AA microwires, which is consistent with the results of Fig. 6(a) and (c), and Table 1.

The fractured surfaces of the studied AA microwires after fracture were further examined to gain deeper insights into their deformation and fracture mechanism. Fig. 7(a)-(l) show the surface morphologies of these AA microwires after fracture at 1×10^{-2} s^{-1}. The studied AA microwire exhibits a shear fracture angle of 56.8° between the applied stress axis and the fractured surface (See

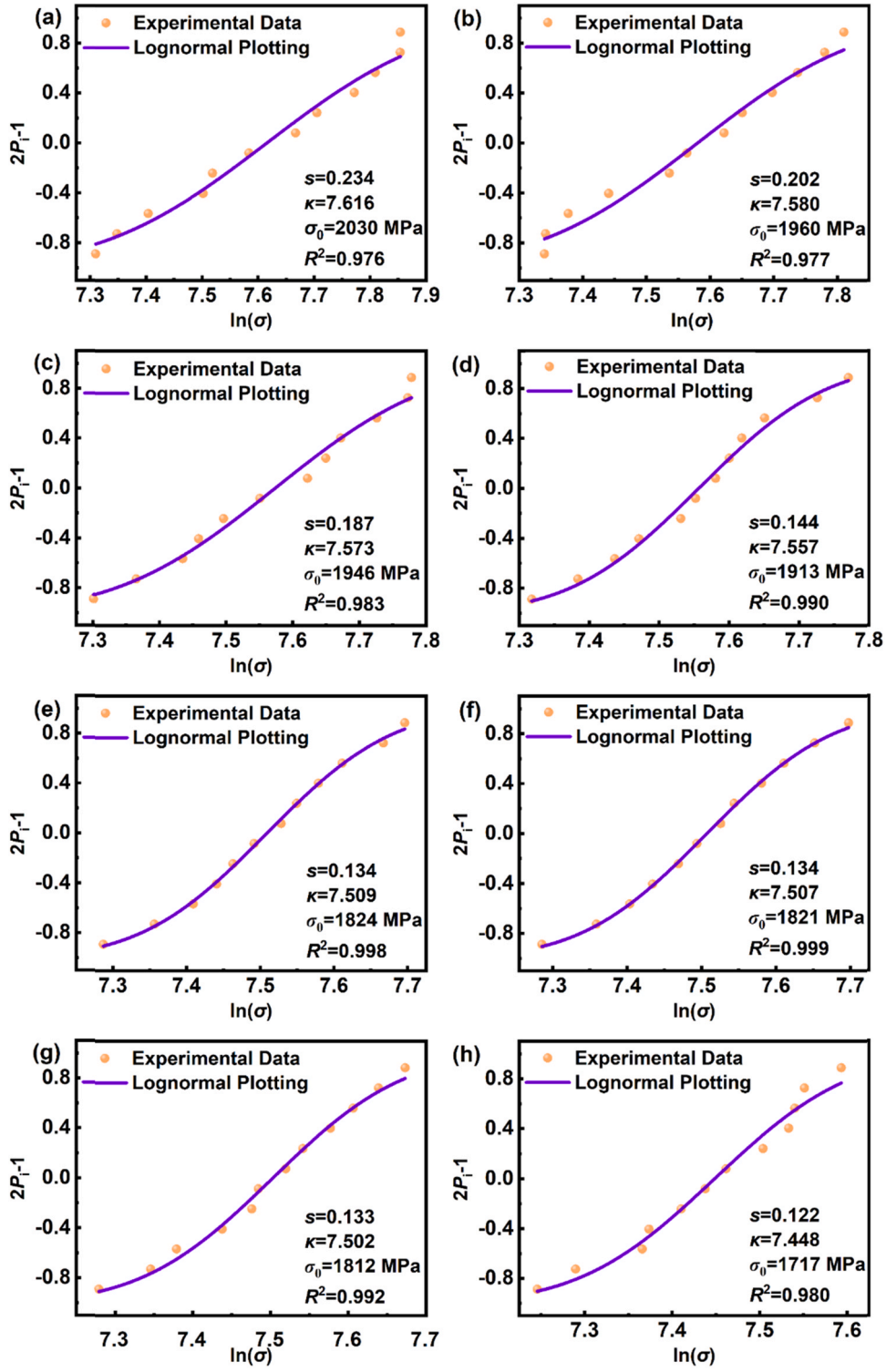

Fig. 4. Lognormal distribution fitting curves of $Cu_{45}Zr_{45}Co_{10}$ AA microwires under different strain rates of (a) 5×10^{-2} s^{-1}, (b) 1×10^{-2} s^{-1}, (c) 5×10^{-3} s^{-1}, (d) 1×10^{-3} s^{-1}, (e) 5×10^{-4} s^{-1}, (f) 1×10^{-4} s^{-1}, (g) 5×10^{-5} s^{-1} and (h) 1×10^{-5} s^{-1}, respectively. The insets display the corresponding fitting parameters.

Fig. 7(a) inset). The fracture angles at other fracture strength and other strain rates are 55–58°, which are measured from SEM images (not shown here). The sheared-off angle was almost unaffected by the strain rate or fracture strength, which obeyed the Mohr-Coulomb criterion [40,41]. Upon the formation of this fracture, it propagates uniformly and this result corroborates the results given in Fig. 3(a)-(h). It has been shown that the shear fracture is the main fracture mechanism of $Cu_{45}Zr_{45}Co_{10}$ AA microwires [42].

The fracture surfaces of the studied AA microwires show two well-defined regions, i.e., vein-like area and smooth shear offset area (separated by dashed lines in Fig. 7(b)). Typical vein-like patterns have been explained well by Saffman Taylor flow instability of the crack front [43]. The patterns induced by flow instability strongly suggest that the failures are triggered by shear. The shearing force in the tensile deformation process causes friction between the parallel layers of AA microwires. At the moment of fracture, the energy

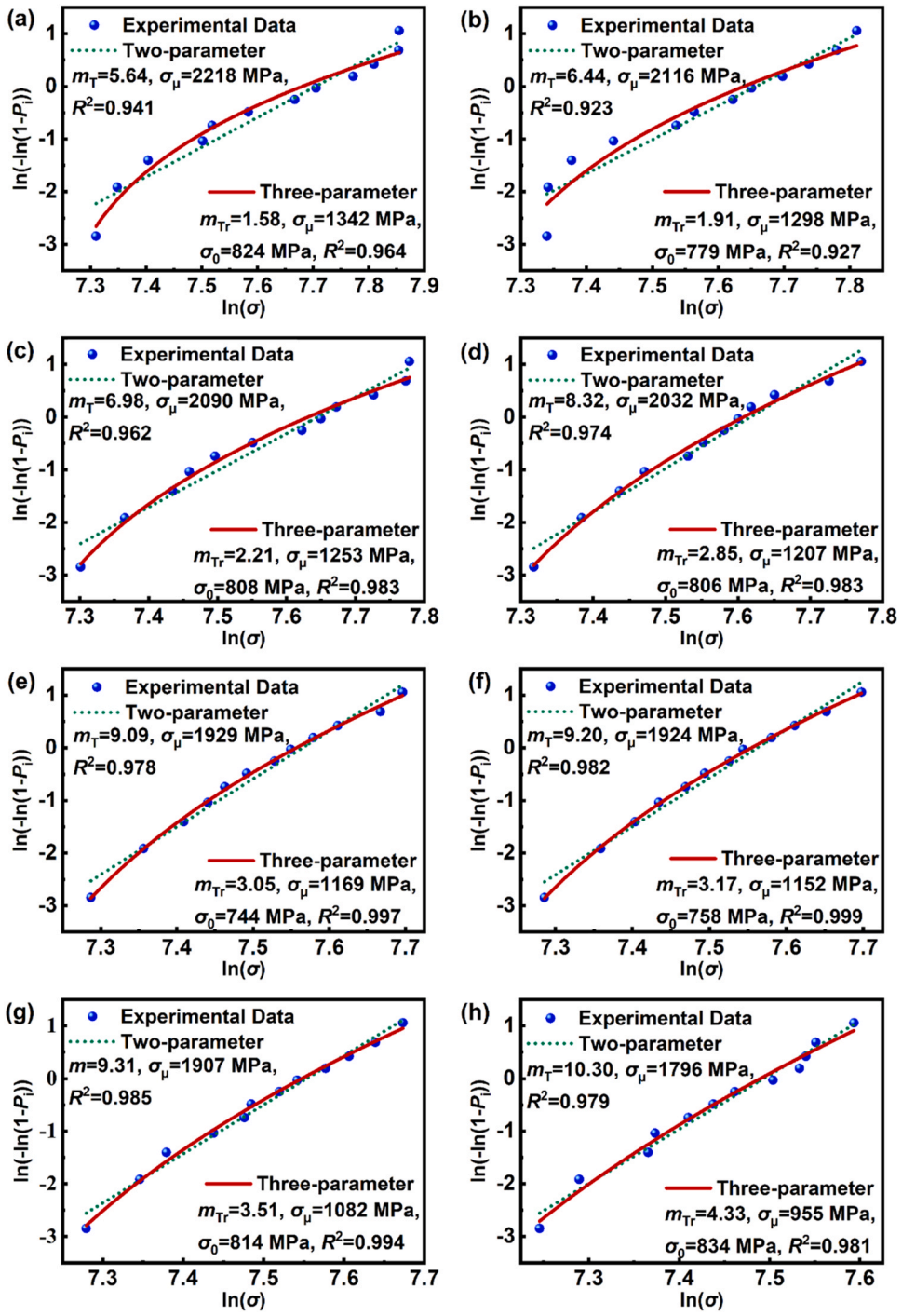

Fig. 5. Two- and three-parameter Weibull distribution fitting curves of $Cu_{45}Zr_{45}Co_{10}$ AA microwires under different strain rates of (a) 5×10^{-2} s^{-1}, (b) 1×10^{-2} s^{-1}, (c) 5×10^{-3} s^{-1}, (d) 1×10^{-3} s^{-1}, (e) 5×10^{-4} s^{-1}, (f) 1×10^{-4} s^{-1}, (g) 5×10^{-5} s^{-1} and (h) 1×10^{-5} s^{-1}, respectively. The insets display the corresponding fitting parameters.

accumulated by the stress of the AA microwire is released quickly, accompanied by adiabatic heating, resulting in partial melting, shear dilatation and the viscosity of the AA microwire dropping, resulting in the formation of vein-like patterns [44]. The mirror-like shear offset area is very smooth and featureless, where rapid fracture deformation eventually occurs. It has been accepted that these shear offset areas correspond to local nucleation sites of the crack because of the normal tensile stress on the fracture surface [45,46]. Therefore, the smooth shear offset and vein-like areas are generally considered to be crack nucleation and crack propagation regions, respectively. Meanwhile, the local temperature rise leads to some micro-areas melt, and the molten metal splashes and forms molten droplets at the moment of fracture, as is shown by the arrow in Fig. 7(k).

The two regions on fracture surfaces of AA microwires are found to be closely related to fracture strength values. A typical tensile rate of 1×10^{-5} s^{-1} is taken as an example, and a series of fracture surfaces images are shown in Fig. 7(a)-(l). A sharp contrast between the densities of vein-like pattern and the length of shear offset area is also evident. An increase in fracture strength resulted in a more intensive vein-like pattern in the fracture surface. This is because higher fracture strength means the more strain energy stored in the materials, leading to the formation of higher number and density of veins at the moment of fracture [47]. Besides, as shown in Fig. 7(a),

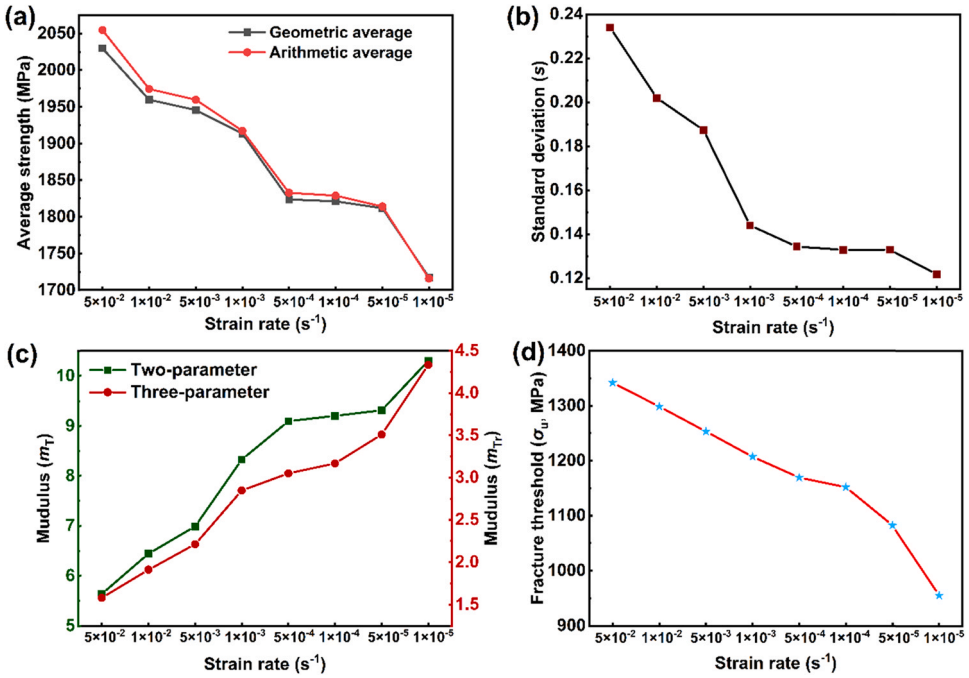

Fig. 6. Fitting parameters of lognormal as well as two- and three-parameter Weibull distribution models of $Cu_{45}Zr_{45}Co_{10}$ AA microwires under different strain rates. (a) Fracture strengths of arithmetic average values and geometric average values, (b) standard deviations calculated by lognormal distribution, (c) modulus of two- and three-parameter Weibull distribution, and (d) fracture threshold values of two-parameter Weibull distribution.

the shear offset length is ~24 μm while fracture strength is 1540 MPa. When fracture strength increases to 2467 MPa, the shear offset length reduces to ~7 μm. For other strain rates, the fracture strength value and shear offset length of each specimen are listed in Table 1. As seen, at each strain rate, the shear offset length of AA microwire decreases with the increase of fracture strength values. It is suggested that fracture strength has a significant effect on fracture surface morphology, especially the length of shear offset.

In order to clarify the effect of fracture strength on shear offset length, it is necessary to explain the above fracture phenomenon in more details. Based on characteristic of brittle materials, the applied maximum stress during tensile process should not exceed the

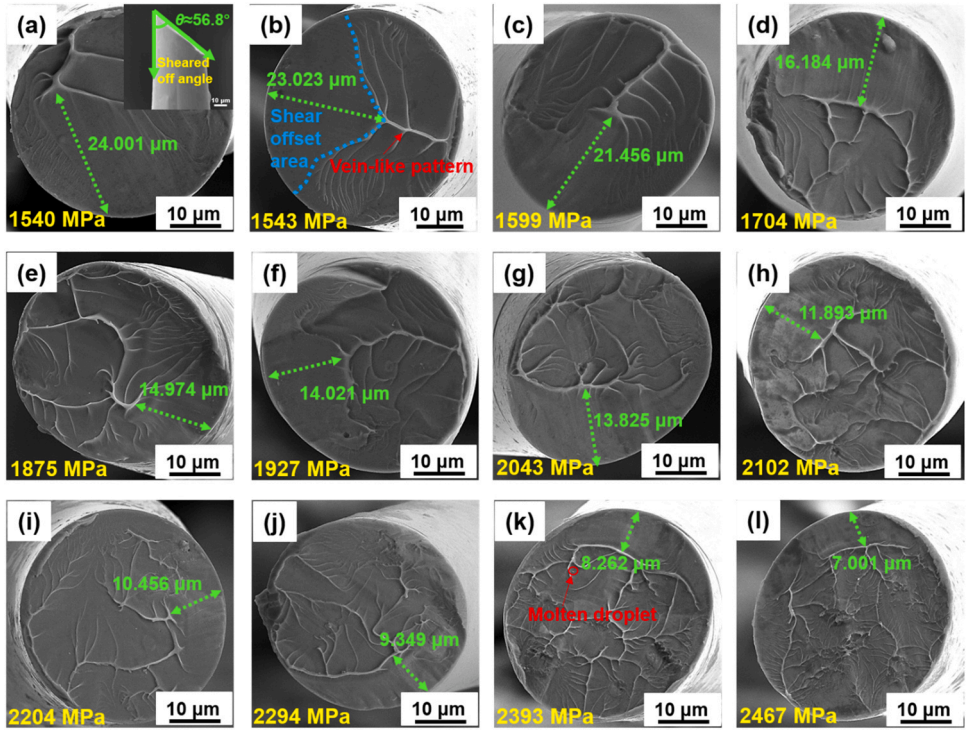

Fig. 7. SEM images of $Cu_{45}Zr_{45}Co_{10}$ AA microwires after fracture under strain rates of 1.0×10^{-2} s^{-1} with different fracture strengths of (a) 1540 MPa, (b) 1543 MPa, (c) 1599 MPa, (d) 1704 MPa, (e) 1875 MPa, (f) 1927 MPa, (g) 2043 MPa, (h) 2102 MPa, (i) 2204 MPa, (j) 2294 MPa, (k) 2393 MPa, and (l) 2467 MPa, respectively.

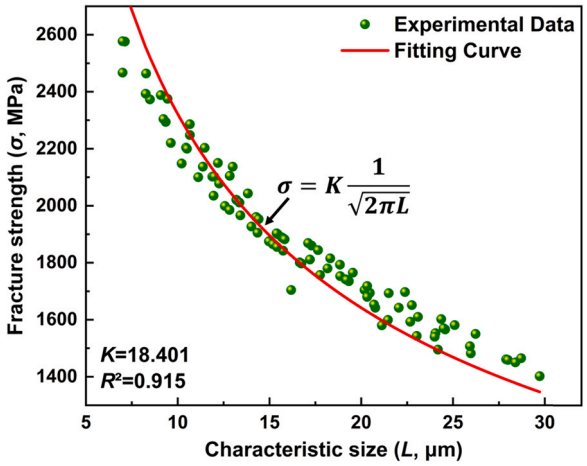

Fig. 8. Fracture strength σ of $Cu_{45}Zr_{45}Co_{10}$ AA microwires as a function of the characteristic length L of shear offset regions under different strain rates from 5×10^{-2} s^{-1} to 1×10^{-5} s^{-1}, indicating a scaling law between σ and L that is described well by Eq. (1). The insets show corresponding parameters.

fracture strength. In applying an approach based on fracture mechanics, the structure cannot be assumed to be defect-free. Rather, an initial crack must be assumed. Griffith [48] suggested that internal tiny flaws can act as stress raisers in solids, thus strongly affecting their tensile strengths. According to the linear elastic fracture mechanics, fracture is governed by $K \le K_C$, where K is a measure of the stress singularity at the tip of the crack and K_C is the critical value of K.

According to classical fracture mechanics [49], brittle fracture of materials is sensitive to the crack nucleation process, which directed us to examine the nucleation regions of cracks, i.e., shear offset areas. We measured the length of shear offset areas of all fractured specimens, and plotted these sizes against the macroscopic fracture strengths in Fig. 8. Interestingly, the scattered fracture strengths show a direct correlation with the shear offset lengths. Further analysis uncovers a scaling law between the fracture strength σ and the characteristic size L of shear offset area length, which can be expressed by

$$\sigma = K\frac{1}{\sqrt{2\pi L}} \tag{12}$$

Eq. (12) means that linear elastic fracture mechanics can describe well the tensile fracture strength of AA microwires that is governed by the crack nucleation process corresponding to different degrees of stress concentrations. In this case, the parameter K can be regarded as the stress intensity factor. As the characteristic length of shear offset area decreases, fracture strength increases. It is proved that the dispersive L values lead to the dispersion of fracture strength values as the strain rate increases from 1×10^{-5} s^{-1} to 5×10^{-2} s^{-1}, vice versa. The square root singularity of the characteristic lengths of shear offset on fracture surfaces reasonably explains the above results that the fracture reliability of the studied AA microwires increases with the decrease of the applied strain rate.

5. Conclusion

In summary, the effect of the applied strain rate on the mechanical properties of $Cu_{45}Zr_{45}Co_{10}$ AA microwires was investigated. The following conclusions can be drawn:

1. According to lognormal as well as two- and three-parameter Weibull statistics, both geometric and arithmetic average fracture strength values, and fracture threshold values show positive sensitivity to the applied strain rate of $Cu_{45}Zr_{45}Co_{10}$ AA microwires.
2. The main fracture mode of $Cu_{45}Zr_{45}Co_{10}$ AA microwires during the tensile test is shear fracture. The increasing fracture strength is accompanied by an increase in the length of shear offset area and a more intensive vein-like pattern.
3. An increasing trend of the fracture reliability has been discovered as the applied strain rate decreases from 5.0×10^{-2} s^{-1} to 1.0×10^{-5} s^{-1}. The fracture reliability is dominated by a square root singularity of shear offset lengths on fracture surfaces.

CRediT authorship contribution statement

Z.L.N., S.S., M.Q.J., S.D.J, and Y.J.H. proposed idea and wrote manuscript, S.S., and K.Y.W. prepared the samples, S.S., and K.Y.W. carried out the experiments, S.S., Z.L.N., Y.J.H., T.Y., K.Y.W., M.Q.J., J.F.S., and S.D.J. revised and corrected the manuscript, S.S., and K.Y.W. analyzed the data. All authors discussed the results and reviewed the manuscript.

Declaration of Competing Interest

The authors declare that they have no known competing financial interests or personal relationships that could have appeared to influence the work reported in this paper.

Acknowledgement

This work was financially supported by the Natural Science Foundation of China (NSFC, No. 52071118, 51901057, and 52171154) and China Postdoctoral Science Foundation (Nos. 2019M661275 and 2020T130030ZX). M.Q. Jiang acknowledges the support of National Outstanding Youth Science Fund Project (No. 12125206) of NSFC.

References

[1] J. Schroers, W.L. Johnson, Ductile bulk metallic glass, Phys. Rev. Lett. 93 (25) (2004) 255506.
[2] J. Li, F. Spaepen, T. Hufnagel, Nanometre-scale defects in shear bands in a metallic glass, Philos. Mag. A 82 (13) (2002) 2623–2630.
[3] H. Zhang, H. Sun, S. Pan, D. Şopu, C. Peng, K. Zhao, K. Song, S. Yuan, J. Qiao, L. Wang, J. Eckert, Origin of structural heterogeneity in Zr-Co-Al metallic glasses from the point of view of liquid structures, J. Non-Cryst. Solids 553 (2021) 120501.
[4] D. Şopu, S. Scudino, X. Bian, C. Gammer, J. Eckert, Atomic-scale origin of shear band multiplication in heterogeneous metallic glasses, Scr. Mater. 178 (2020) 57–61.
[5] S. Wu, Z. Liu, R. Qu, Z. Zhang, Designing metallic glasses with optimal combinations of glass-forming ability and mechanical properties, J. Mater. Sci. Technol. 67 (2021) 254–264.
[6] H. Shen, L. Luo, Y. Bao, H. Yin, S. Jiang, L. Zhang, Y. Huang, S. Feng, D. Xing, J. Liu, New DyHoCo medium entropy amorphous microwires of large magnetic entropy change, J. Alloy. Compd. 837 (2020) 155431.
[7] D. Estevez, Y. Zhao, Y. Wang, F. Qin, H.-X. Peng, Optimizing magnetoimpedance of amorphous microwires by nanocarbon-induced magnetic anisotropy, J. Magn. Magn. Mater. 502 (2020) 166527.
[8] M. Nematov, I. Baraban, N. Yudanov, V. Rodionova, F. Qin, H.-X. Peng, L. Panina, Evolution of the magnetic anisotropy and magnetostriction in Co-based amorphous alloys microwires due to current annealing and stress-sensory applications, J. Alloy. Compd. 837 (2020) 155584.
[9] J. Onufer, J. Ziman, P. Duranka, M. Kladivová, The influence of annealing on domain wall propagation in bistable amorphous microwire with unidirectional effect, Phys. B: Condens. Matter 540 (2018) 58–64.
[10] K. Chichay, V. Rodionova, V. Zhukova, M. Ipatov, N. Perov, M. Gorshenkov, N. Andreev, A. Zhukov, Tunable domain wall dynamics in amorphous ferromagnetic microwires, J. Alloy. Compd. 835 (2020) 154843.
[11] Y.B. Wang, C.C. Lee, J. Yi, X.H. An, M.X. Pan, K.Y. Xie, X.Z. Liao, J.M. Cairney, S.P. Ringer, W.H. Wang, Ultrahigh-strength submicron-sized metallic glass wires, Scr. Mater. 84–85 (2014) 27–30.
[12] H. Yin, Y. Huang, D. Daisenberg, P. Xue, S. Jiang, W. Ru, S. Jiang, Y. Bao, X. Bian, X. Tong, H. Shen, J. Sun, Atomic structure evolution of high entropy metallic glass microwires at cryogenic temperature, Scr. Mater. 163 (2019) 29–33.
[13] I. Alekhina, V. Kolesnikova, A. Komlev, M. Khajrullin, L. Makarova, V. Rodionova, N. Perov, Radial dependence of circular magnetic permeability of amorphous magnetic microwires, J. Magn. Magn. Mater. (2021) 168155.

[14] X. Bian, G. Wang, Q. Wang, B. Sun, I. Hussain, Q. Zhai, N. Mattern, J. Bednarčík, J. Eckert, Cryogenic-temperature-induced structural transformation of a metallic glass, Mater. Res. Lett. 5 (4) (2016) 284–291.
[15] J. Dong, Y.-H. Feng, Y. Huan, J. Yi, W.-H. Wang, H.-Y. Bai, B.-A. Sun, Rejuvenation in hot-drawn micrometer metallic glassy wires, Chin. Phys. Lett. 37 (1) (2020) 017103.
[16] H. Yang, K. Cao, Y. Han, M. Wen, J. Guo, Z. Tan, J. Lu, Y. Lu, The combined effects of grain and sample sizes on the mechanical properties and fracture modes of gold microwires, J. Mater. Sci. Technol. 35 (1) (2019) 76–83.
[17] B. Zberg, E.R. Arata, P.J. Uggowitzer, J.F. Löffler, Tensile properties of glassy MgZnCa wires and reliability analysis using Weibull statistics, Acta Mater. 57 (11) (2009) 3223–3231.
[18] J. Zhang, D. Estévez, Y.-Y. Zhao, L. Huo, C. Chang, X. Wang, R.-W. Li, Flexural strength and weibull analysis of bulk metallic glasses, J. Mater. Sci. Technol. 32 (2) (2016) 129–133.
[19] F.X. Qin, N.S. Bingham, H. Wang, H.X. Peng, J.F. Sun, V. Franco, S.C. Yu, H. Srikanth, M.H. Phan, Mechanical and magnetocaloric properties of Gd-based amorphous microwires fabricated by melt-extraction, Acta Mater. 61 (4) (2013) 1284–1293.
[20] W. Zheng, Y. Huang, G. Wang, P. Liaw, J. Shen, Influence of strain rate on compressive deformation behavior of a Zr-Cu-Ni-Al bulk metallic glass at room temperature, Metall. Mater. Trans. A 42 (6) (2011) 1491–1498.
[21] W. Ma, H. Kou, J. Li, H. Chang, L. Zhou, Effect of strain rate on compressive behavior of Ti-based bulk metallic glass at room temperature, J. Alloy. Compd. 472 (1–2) (2009) 214–218.
[22] J. Zhang, J.M. Park, D.H. Kim, H.S. Kim, Effect of strain rate on compressive behavior of Ti45Zr16Ni9Cu10Be20 bulk metallic glass, Mater. Sci. Eng. A 449 (2007) 290–294.
[23] J. Sort, J. Fornell, W. Li, S. Surinach, M. Baró, Influence of the loading rate on the indentation response of Ti-based metallic glass, J. Mater. Res. 24 (3) (2009) 918–925.
[24] Y. Ma, J. Ye, G. Peng, D. Wen, T. Zhang, Nanoindentation study of size effect on shear transformation zone size in a Ni–Nb metallic glass, Mater. Sci. Eng. A 627 (2015) 153–160.
[25] T. Burgess, K. Laws, M. Ferry, Effect of loading rate on the serrated flow of a bulk metallic glass during nanoindentation, Acta Mater. 56 (17) (2008) 4829–4835.
[26] Z. Mao, X. An, X. Liao, J. Wang, Opposite grain size dependence of strain rate sensitivity of copper at low vs high strain rates, Mater. Sci. Eng.: A 738 (2018) 430–438.
[27] Y. Wu, H.H. Wu, X.D. Hui, G.L. Chen, Z.P. Lu, Effects of drawing on the tensile fracture strength and its reliability of small-sized metallic glasses, Acta Mater. 58 (7) (2010) 2564–2576.
[28] W.-B. Liao, C. Jiang, S. Xu, L. Gao, H. Zhang, P. Li, Z. Liu, Y. Lu, Reliability of tensile fracture strength of Co-based metallic glass microwires by Weibull statistics, Mater. Res. Express 6 (10) (2019) 106565.
[29] K. Tao, J. Qiao, Q. He, K. Song, Y. Yang, Revealing the structural heterogeneity of metallic glass: Mechanical spectroscopy and nanoindentation experiments, Int. J. Mech. Sci. 201 (2021) 106469.
[30] X.L. Bian, D. Zhao, J.T. Kim, D. Şopu, G. Wang, R. Pippan, J. Eckert, Controlling the distribution of structural heterogeneities in severely deformed metallic glass, Mater. Sci. Eng.: A 752 (2019) 36–42.
[31] P. Liu, L. Wang, Y. Yue, S. Song, X. Wang, K.M. Reddy, X. Liao, Z. Zhang, M. Chen, X. Han, Room-temperature superplasticity in Au nanowires and their atomistic mechanisms, Nanoscale 11 (18) (2019) 8727–8735.
[32] J. Liu, M. Pang, G. Cao, G. Qu, X. Wang, Y. Zhang, R. Liu, H. Shen, Comparative study of tensile properties and magnetic properties for Nb-doped Fe-based wires, J. Mater. Res. Technol. 9 (6) (2020) 12907–12916.
[33] Y.J. Chen, X.H. An, X.Z. Liao, Mechanical behaviors of nanowires, Appl. Phys. Rev. 4 (2017) 031104.
[34] W.H. Wang, Correlations between elastic moduli and properties in bulk metallic glasses, J. Appl. Phys. 99 (9) (2006) 093506.
[35] N. Duc, H. Shen, O. Thiabgoh, N. Huong, J. Sun, M. Phan, Melt-extracted Gd73.5Si13B13. 5/GdB6 ferromagnetic/antiferromagnetic microwires with excellent magnetocaloric properties, J. Alloy. Compd. 818 (2020) 153333.
[36] W. Sharpe, J. Pulskamp, D. Gianola, C. Eberl, R. Polcawich, R. Thompson, Strain measurements of silicon dioxide microspecimens by digital imaging processing, Exp. Mech. 47 (5) (2007) 649–658.
[37] Z. Han, L. Tang, J. Xu, Y. Li, A three-parameter Weibull statistical analysis of the strength variation of bulk metallic glasses, Scr. Mater. 61 (9) (2009) 923–926.
[38] J. Sullivan, P. Lauzon, Experimental probability estimators for Weibull plots, J. Mater. Sci. Lett. 5 (12) (1986) 1245–1247.
[39] A. Argon, Plastic deformation in metallic glasses, Acta Metall. 27 (1) (1979) 47–58.
[40] C.A. Schuh, A.C. Lund, Atomistic basis for the plastic yield criterion of metallic glass, Nat. Mater. 2 (7) (2003) 449–452.
[41] J. Caris, J. Lewandowski, Pressure effects on metallic glasses, Acta Mater. 58 (3) (2010) 1026–1036.
[42] H. Wang, F.X. Qin, D.W. Xing, F.Y. Cao, X.D. Wang, H.X. Peng, J.F. Sun, Relating residual stress and microstructure to mechanical and giant magneto-impedance properties in cold-drawn Co-based amorphous microwires, Acta Mater. 60 (15) (2012) 5425–5436.
[43] P.G. Saffman, G.I. Taylor, The penetration of a fluid into a porous medium or Hele-Shaw cell containing a more viscous liquid, Proc. R. Soc. Lond. Ser. A Math. Phys. Sci. 245 (1242) (1958) 312–329.
[44] K.M. Flores, R.H. Dauskardt, Local heating associated with crack tip plasticity in Zr–Ti–Ni–Cu–Be bulk amorphous metals, J. Mater. Res. 14 (3) (1999) 638–643.
[45] Z. Zhang, J. Eckert, L. Schultz, Difference in compressive and tensile fracture mechanisms of Zr59Cu20Al10Ni8Ti3 bulk metallic glass, Acta Mater. 51 (4) (2003) 1167–1179.
[46] R. Qu, M. Stoica, J. Eckert, Z. Zhang, Tensile fracture morphologies of bulk metallic glass, J. Appl. Phys. 108 (6) (2010) 063509.
[47] Z. Lu, C. Liu, J. Thompson, W. Porter, Structural amorphous steels, Phys. Rev. Lett. 92 (24) (2004) 245503.
[48] V.E. Saouma (Ed.), Cornell University, 1981.
[49] M.Q. Jiang, G. Wilde, J.H. Chen, C.B. Qu, S.Y. Fu, F. Jiang, L.H. Dai, Cryogenic-temperature-induced transition from shear to dilatational failure in metallic glasses, Acta Mater. 77 (2014) 248–257.